Chemical Physics 165 (1992) 173–182
North-Holland

Two-photon dissociation of SO_2 in the ultraviolet region

Tetsuya Sato, Tohru Kinugawa, Tatsuo Arikawa
Department of Applied Physics, Faculty of Engineering, Tokyo University of Agriculture and Technology, Koganei 184, Japan

and

Masahiro Kawasaki
Institute of Electronics Science, Hokkaido University, N12W6, Sapporo 060, Japan

Received 17 June 1991; in final form 9 April 1992

Two-photon photodissociation of SO_2 through the $\tilde{B}\ ^1B_1$ state at 286–309 nm has been studied by a perfect focusing mass spectroscopy and a photofragment imaging technique. Sulfur atoms were detected as photofragments by a resonance-enhanced multiphoton ionization technique. The lower limits of the anisotropy parameters for angular distributions are 0.42 ± 0.06 for $S(^1D)$ and 0.50 ± 0.05 for $S(^3P)$. The velocity distributions of the $S(^1D$ and $^3P)$ photofragments are analyzed assuming dissociation pathways: $SO_2 + 2\hbar\omega \rightarrow S(^1D$ and $^3P) + O_2(a\ ^1\Delta$ and $X\ ^3\Sigma_g^-)$. The two-photon excited state of SO_2 around the 8 eV region is assigned to be $\tilde{B}\ ^1B_1$ with C_{2v} symmetry.

1. Introduction

When sufficient amount of energy is put into an SO_2 molecule by a two-photon absorption, dissociation takes place into an $S(^1D$ or $^3P)$ atom and an O_2 molecule as well as an SO molecule and an O atom [1–3]. It has previously been shown that at 193 nm one-photon dissociation exclusively leads to SO + O [4,5] but at the shorter wavelengths, 123.6 (10.0 eV) and 147.0 nm (8.4 eV), dissociation to $S + O_2$ was also found [6],

$$SO_2 \rightarrow SO(X\ ^3\Sigma_g^-) + O(^3P \text{ or } ^1D)\ ,$$
$$\Delta H = 5.7 \text{ or } 7.7 \text{ eV}\ ,$$
$$\rightarrow S(^3P \text{ or } ^1D) + O_2(X\ ^3\Sigma_g^-)\ ,$$
$$\Delta H = 5.9 \text{ or } 7.0 \text{ eV}\ ,$$
$$\rightarrow S(^3P \text{ or } ^1D) + O_2(a\ ^1\Delta)\ ,$$
$$\Delta H = 6.9 \text{ or } 8.0 \text{ eV}\ .$$

Correspondence to. M. Kawasaki, Institute of Electronics Science, Hokkaido University, N12W6, Sapporo 060, Japan

Wilson et al. [1] and Venkitachalam and Bersohn [2] reported in their emission and laser induced-fluorescence study that two-photon absorptions at 248 nm and 285–311 nm produce $S(^3P)$ and $S(^1D)$ atoms as well as SO molecules as primary products. Effenhauser et al. [3] reported two-photon absorption of SO_2 at 248 and 308 nm. Their kinetic energy measurement by time-of-flight spectra showed formation of S atoms via the $S + O_2$ process.

Left unanswered are two questions. First, what symmetry does the molecule have after the sequential absorption of two photons that reach the energy region of vacuum UV photon? Second, what dynamics govern the dissociation processes? To answer these questions, both angular and energy resolved data are required for the photofragments. With perfect focusing mass spectroscopy, angular distributions of photofragments have been previously measured for multiphoton dissociation processes; NO molecules from NO_2 [7], sulfur atoms from CS_2 [8], and CH_3^+ ions from CH_3I [9]. Chandler and co-workers [10] have demonstrated that the photofragment imaging technique is very powerful for simultaneous observation of both angular and velocity distributions of photo-

fragments. In this paper, we have applied these techniques to study of two-photon dissociation of SO_2 at the ultraviolet region.

2. Experimental

2.1. Photofragment imaging

Fig. 1 shows the experimental setup of our two-dimensional photofragment imaging. This technique is similar to the photofragment imaging technique reported by Chandler and co-workers [10]. Experimental details are described elsewhere [11]. A polarized UV laser beam (frequency doubled by a BBO crystal, <0.1 mJ/pulse, 0.3 cm^{-1}) focused with a quartz lens ($f=200$ mm) propagates along the Y axis, dissociates parent molecules, and also ionizes photofragments by a multiphoton ionization process. The ions produced by the laser beam are then pulled into a plane, at a certain distance from the ionization center, by an electric field. The masses of ions are separated by their time-of-flight spectra. The image of the ions on the XY plane is detected by a multichannel plate. If the photofragments are monoenergetic, the image will have an outer edge of radius r given by $r=v_{XY}t=(v_X^2+v_Y^2)^{1/2}t$ where t is the time of flight.

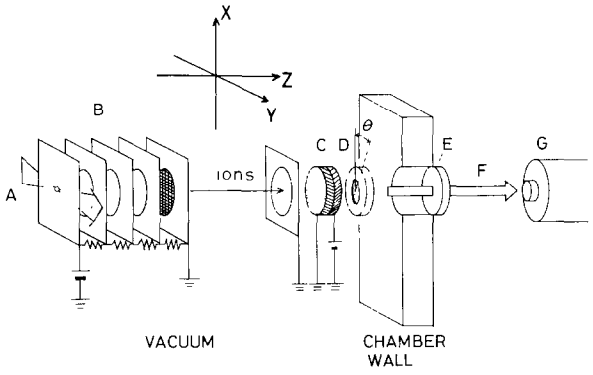

Fig. 1. Schematics of two-dimensional photofragment spectrometer. A nozzle of SO_2 effusive beam lies along detector (z) axis. (A) Focused laser beam for both dissociation of SO_2 and detection of photofragments by resonant-enhanced multiphoton ionization. (B) Acceleration electrodes. (C) Multichannel plates. (D) Phosphor screen. (E) Window for the vacuum chamber. (F) Two-dimensional image. (G) CCD camera with a gated image-intensifier.

The dependence of the intensity of the image on the polar angle θ gives the angular distribution of the photofragments. The image intensity projected on the magic angle axis is independent of the angular distribution of photofragments while it contains information of the translational energy distribution of the photofragments. In this way it is possible to record, at one time, the two-dimensional velocity distribution of a state-selected photofragment.

After the photofragments are selectively ionized for a given internal state, they are directed through an acceleration zone (86 mm long) with four electrodes and then into a time-of-flight tube (500 mm long). The acceleration voltage is typically 1.6 kV. The detector consists of a microchannel plate assembly (Hamamatsu, F1217-03, 40 mm diameter) backed by a phosphor plastic screen (50 ns lifetime). For high resolution mass spectroscopy, a fast phosphor (<5 ns) is used. When taking an image, a gated image intensifier (Hamamatsu, C2925S-2, 3 ns resolution) is used to detect only the ions of interest. By opening the shutter on the detector for variable periods of time, the signals are averaged typically for 3k laser shots through a CCD camera (Sony, XC-77CE). In order to test energy resolution of our imaging spectrometer, thermal nitric oxide in an effusive beam is ionized by a (2+1) resonance enhanced multiphoton ionization technique [11]. The obtained image of NO, $\gamma(0, 0)$ at 226.3 nm has a diameter of 0.74 mm small enough to assure spacial resolution.

Sulfur dioxide (Matheson) was introduced into a vacuum chamber through an effusive molecular beam with a stainless steel nozzle. The pressure of the chamber was maintained at 8×10^{-6} Torr during operation. In this one-color laser experiment, the linearly (X) polarized UV laser light was focused at 2 mm below the nozzle and used both as a dissociation laser and a probe one. For the measurement of 2D photofragment images, the laser intensity was reduced until only a few tens of ions were detected per laser shot in order to eliminate (a) the saturation effect, (b) the space charge effect among the ions produced, and (c) additional multiphoton processes. The two-photon resonant enhanced three-photon ionization (REMPI) signals of sulfur atoms were observed at 286–309 nm as listed in table 1. The flat background signals are subtracted from the imagings which are to be analyzed.

Table 1
Anisotropy parameter for angular distribution, maximum and averaged translational energies of S atoms from two-photon dissociation of SO_2 in one-color UV laser experiment

λ(nm) [a]	Two-photon transition of S atoms	β_2 [b]	E_T(S)(eV)	
			max. [c]	averaged [d]
288.19 [e),f)]	$4\,^1F_3$–$3\,^1D$	0.40±0.05	–	–
291.24 [e)]	$6\,^3P_1$–$3\,^1D$	0.44±0.05	–	–
291.49 [e),f)]	$4\,^1P_1$–$3\,^1D$	0.42±0.05	0.28±0.05	0.09
308.20 [f)]	$4\,^3P_2$–$3\,^3P_2$	0.50±0.05	0.70±0.05	0.21

[a] Laser wavelength for two-photon dissociation of SO_2 and (2+1) resonance-enhanced multiphoton-ionization probing of S atoms.
[b] An anisotropy parameter for eq. (1). These values are lower limits (see text).
[c] Maximum translational energy of S atoms from fig. 5.
[d] Averaged translational energy of S atoms from fig. 5.
[e] Experimental results by perfect focusing mass spectroscopy. Assignment is taken from ref. [28].
[f] Experimental results by a photofragment imaging technique.

2.2. Perfect focusing mass spectroscopy

By means of a canonical transformation, Iwata [12] has shown that a perfect three-dimensional focusing field is realized by the use of a combination of an electrostatic and an uniform magnetic field. Once the ions are scattered from the interaction point of the molecule and the focused laser light, all charged particles of the same effective mass converge perfectly to a focusing point (detection point) independent of the initial velocity vector. Our home-made mass spectrometer used to obtain mass spectra and angular distributions is identical with that reported previously [13]. In brief, the polarized light pulse from an excimer laser-pumped dye laser was focused on an effusive beam of SO_2 by an $f=150$ mm lens. The effusive beam emerged through a needle of 0.3 mm diameter. The vacuum vessel was pumped by a diffusion pump to a base pressure of 10^{-6} Torr.

By changing the electric field strength, we obtain mass spectra. For the measurement of angular distributions, a cone-type collimator is placed in front of the detector. The dimensions of the collimator are diameter=0.7 mm and length=2.0 mm, and it has a half-angle of 10° for a detector (Spiraltron, Galileo). Monitoring the signal intensity of positive ions, the angular distribution was obtained by rotating the electric vector of the laser light with respect to the effective detector direction.

3. Results

3.1. Formation of sulfur atoms in the ^3P and ^1D levels

Since SO_2 has substantial photoabsorption in the UV region, photodissociation takes place by the UV probe laser light itself. Photofragment sulfur atoms in the ^3P or ^1D level are ionized by the same laser light. Firstly, the $m/e=32$ ions are collected in the perfect focusing mass spectrometer as a function of the probe laser wavelength. The $m/e=32$ ions are also observed by the photofragment imaging technique. Strong signals are observed at 288.19 and 308.20 nm, which are identified as belonging to the transitions from $S(3\,^1D)$ and $S(3\,^3P_2)$ to the two-photon allowed states, respectively,

$$S(3\,^1D)\xrightarrow{2\hbar\omega}S(4\,^1F_3, 4\,^3P_1, 4\,^1P_1)\xrightarrow{\hbar\omega}S^+ ,$$

$$S(3\,^3P_2)\xrightarrow{2\hbar\omega}S(4\,^3P_2)\xrightarrow{\hbar\omega}S^+ .$$

Parts of the spectra are shown in fig. 2, in which the $S(^1D)$ transitions are observed at 288.19, 291.24, and 291.49 nm. $4\,^3P_1$. The source of the sulfur atoms was not the photodissociation of any of the sulfur-containing impurities, which were probably present in SO_2. To test this assertion, OCS gas was introduced into the system and irradiated under identical conditions to those of SO_2. No sulfur ion signals were detected from OCS. Another possibility for produc-

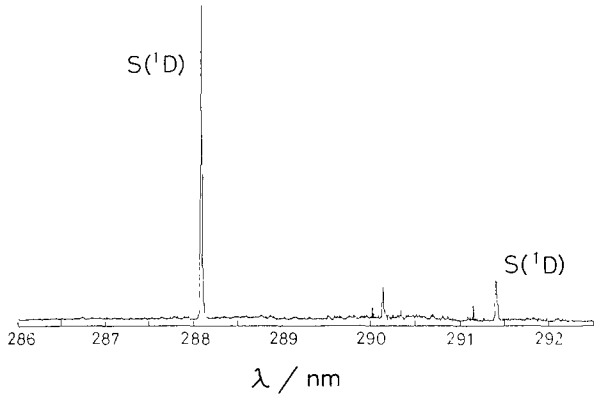

Fig. 2. A part of excitation spectrum of $m/e=32$ signals obtained in two-photon dissociation of SO_2 by a perfect focusing mass spectrometer.

tion of sulfur atoms is the subsequent excitation of $SO(X\,^3\Sigma^-)$ state to the high lying Rydberg states which could predissociate to give $S(^3P)$ and $O(^3P$ and $^1D)$ [14]. Although the ionization potential of SO is 2.6 and 2.1 eV below the energy of three 288 and 308 nm quanta, respectively, no SO^+ signals were observed. Other molecules, in addition to SO_2, could be used as "donors" of SO. Such a molecule is $SOCl_2$, which has an absorption at $\lambda<290$ nm and may dissociate into SO+2Cl [15]. We have observed no REMPI spectra of S atoms when $SOCl_2$ was introduced into the chamber. It is concluded that an SO molecule is not a significant precursor of the S atom. Steadman and Baer [16] reported the formation of $S(^1D)$ and H_2 ($v=10$–14) in two-photon dissociation of H_2S at ≈ 300 nm while no formation of $S(^3P)$ was observed. In our experiment, both $S(^1D)$ and $S(^3P)$ are detected. Hence, H_2S could not be a source of the S atoms. Since neither impurities nor SO are indicated as the principal source of the S atoms, it remains that the sulfur atoms observed must be a primary photoproduct of SO_2.

Here, we consider the possibility of three-body dissociation of SO_2 into S+O+O. For three-body dissociation, three photons at 286–309 nm are needed while two photons are enough for dissociation into $S+O_2$. Furthermore, the laser intensity is reduced so that only a few tens of ions are detected for each laser pulse. This may reduce the possibility of three-photon absorption for the three body dissociation of SO_2. This implies that the excited SO_2 state dissociates mostly through the two-body dissociation; $S+O_2$. Table 2 shows the energetics of these dissociation channels.

Two-dimensional images of the photofragments on the phosphor screen were observed at 291.49 and 308.20 nm for $S(^1D)$ and $S(^3P_2)$ as shown in figs. 3a and 3b, respectively. The shapes of these images are attributed to the energy and angular distributions of photofragments. Fig. 3a for $S(^1D)$ has a smaller diameter than fig. 3b for $S(^3P)$. These spectra are characterized by a maximum intensity along the direction of the electronic vector of the dissociation laser.

In the wavelength range 286–309 nm, when laser intensity was five times increased, weak structured signals were detected in the MPI spectra for the mass number $m/e=32$ along with strong REMPI signals of sulfur atoms. The isotope ratios were measured for the $m/e=32$ signals by the TOF mass spectroscopy. We found that the $m/e=32/33/34$ ratio for these

Table 2
Energetics of dissociation processes of SO_2

Primary process		ΔH (eV) [a]	E_{excess} (eV) [b]	v_{max} [c]
singlet channel	$S(^1D)+O_2(X\,^3\Sigma_g^-)$	7.0	1 5	7
	$S(^1D)+O_2(a\,^1\Delta)$	8.0	0.5	2
triplet channel	$S(^3P)+O_2(X\,^3\Sigma_g^-)$	5.9	2.1	11
	$S(^3P)+O_2(a\,^1\Delta)$	6.9	1.1	6
	$S(^3P)+O_2(b\,^1\Sigma_g^+)$	7.5	0.5	2

[a] Ref. [3].
[b] $2\hbar\omega-\Delta H$ for one-color laser dissociation. $2\hbar\omega$ is 8.5 eV for the singlet channel ($\lambda=291.49$ nm) and is 8.0 eV for the triplet channel ($\lambda=308.20$ nm).
[c] Maximum vibrational quantum numbers of O_2 photofragments.

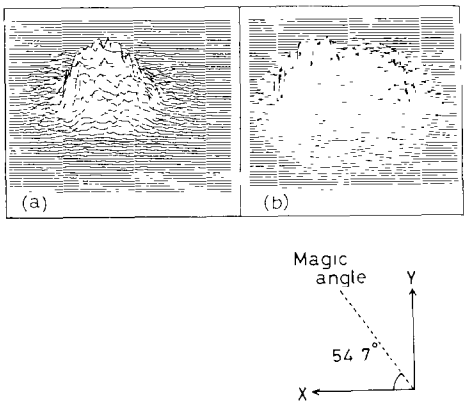

Fig. 3. Two-dimensional images observed at two different laser wavelengths for resonant enhanced (2+1) multiphoton ionization spectra of sulfur photofragments from two-photon dissociation of SO_2. X-axis is along the direction of electric vector of dissociation laser light. (a) $S(^1D)$ at 291.49 nm. (b) $S(^3P)$ at 308.20 nm.

weak signals is 0.96/0.01/0.03 and is the same as for $S(^1D)$ and $S(^3P)$. This ratio is in agreement with the isotopic composition of sulfur atoms (0.9502/0.0075/0.0422) and not with those of oxygen molecules (0.9952/0.0004/0.0020). By higher multiphoton processes, S ions are generated even at off-resonant laser wavelengths. However, contribution of these higher multiphoton processes are quite small in intensity.

3.2. Angular distributions of photofragments observed by perfect focusing mass spectrometry

By choosing appropriate wavelengths for REMPI of $S(^3P_J, ^1D)$, the intensity of S^+ was also measured as a function of the angle θ between the detection axis and the direction of the electric vector of dissociation laser light in the perfect focusing mass spectrometer. An example is shown in fig. 4. The experimentally obtained angular distribution is analyzed, assuming the center-of-mass angular distribution $f(\theta)$ [17],

$$f(\theta) \propto 1 + \beta_2 P_2(\cos\theta) + \beta_4 P_4(\cos\theta) , \qquad (1)$$

where $P_m(\cos\theta)$ is the mth order Legendre polynomial. In order to avoid reduction of the anisotropy by saturation effect, the laser power was reduced until the β value reached an asymptotic value. The curve drawn through the set of data in fig. 4 shows the least-

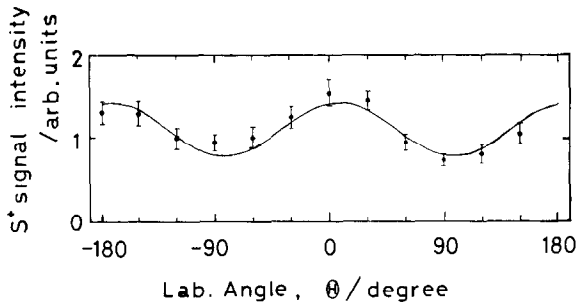

Fig. 4. Angular distribution of $S(^1D)$ photofragments obtained in two-photon dissociation of SO_2 at 291.49 nm by the perfect focusing mass spectrometer. The solid smooth line is a simulated curve of eq. (1) with $\beta_2 = 0.50$ and $\beta_4 = 0$.

squares fit of eq. (1) to the data. Other sets of data were also analyzed by this method. The β_2 value was 0.50 ± 0.05 while the β_4 value was found to be zero for all sets of data. Since this two-photon transition is a sequential two-photon process, the angular distribution reflects only the second one-photoexcitation process. That is why β_4 is zero.

The formation of $S(^1D)$ or $S(^3P)$ from SO_2 is energetically possible at the two-photon energies resonant with the sulfur atomic transitions as listed in table 2. When the complementary photofragment O_2 is vibrationally excited and hence small excess energy is left for the S atom, the anisotropy in the angular distribution may be smeared out because of (a) molecular rotation of the parent molecule, (b) a finite lifetime of the dissociative state, and also (c) mixing of parallel and perpendicular transitions. Hence, the β_2 values obtained from the angular distributions of $S(^1D)$ and $S(^3P)$ are considered to be the lower limits.

3.3. Translational energy and angular distributions of photofragments observed by photofragment imaging method

Images recorded using the photofragment imaging technique are two-dimensional projections of the three-dimensional photofragmentation velocity and angular distributions. The cylindrical symmetry of the velocities around the polarization axis of the photodissociation laser allows one to reconstruct the entire three-dimensional velocity distribution by perform-

ing an inverse Abel transformation [10]. Instead, we performed a best-fit method for data analysis. The images projected on the l axis ($l=X$, Y, or the magic angle) have the angular distribution

$$\frac{dW(u_l)}{du_l} = \frac{1}{u_t}\left[1+\beta_{obs}P_2(\cos\theta')P_2(\cos\theta)\right], \quad (2)$$

where u_l is the velocity vector of a photofragment projected on the l axis, u_t is the velocity of photofragment, and θ' is the angle between the electric vector of the dissociation laser light and the l axis. The image is projected along the magic angle axis that is shown in fig. 3. Since β_4 is zero, the magic angle is defined for the one-photon angular distribution. Putting $\theta'=54.7°$ into eq. (2) eliminates the anisotropy of the photofragments and hence, one can extract the energy distribution from the images projected on the magic angle in a manner analogous to extracting them from the Doppler profile. In our calculation, first we project the images along X and Y axes as shown in fig. 6. Then, we take a sum of one part of the projected images with $\theta'=0°$ and two parts with $\theta'=90°$, that is, $I(\theta'=54.7°)=[I(\theta'=0°)+2I(\theta'=90°)]/3$. The least-squares fit is shown by solid lines in fig. 6 for the images of the $S(^1D)$ and $S(^3P)$ atoms, in which an appropriate β_2 value is assumed, that is, $\beta_2=0.42$ for $S(^1D)$ and 0.50 for $S(^3P)$. Because of the distribution in the images, some errors arise, which are shown in the error bars in fig. 5. As listed in table 1, assuming the $S+O_2$ molecular processes, the maximum total translation energy is 0.56 ± 0.10 eV for the $S(^1D)+O_2$ process, which is in agreement with E_{excess} (0.5 eV) for the formation of $S(^1D)+O_2(a\,^1\Delta)$ and is much lower than E_{excess} (1.5 eV) for $S(^1D)+O_2(X\,^3\Sigma)$ (see table 2). The maximum translational energy for $S(^3P)+O_2$ is 1.4 ± 0.1 eV which is in fair agreement with E_{excess} (1.1 eV) for the $S(^3P)+O_2(a\,^1\Delta)$ process. However, this value is much lower than E_{excess} (2.1 eV) for $S(^3P)+O_2(X\,^3\Sigma_g^-)$. The low translational energy components of the images suggest that the complementary fragment O_2 should be internally excited. Assuming these molecular processes, fig. 5 shows that $P(E_T)$ peaks at low vibrational levels for $O_2(a\,^1\Delta)$ and high vibrational levels for $O_2(X\,^3\Sigma_g^-)$.

With these energy distributions and suitable β_{obs} values, the best-fit curves are calculated for the images projected on the Y axis as in fig. 6 when the angle

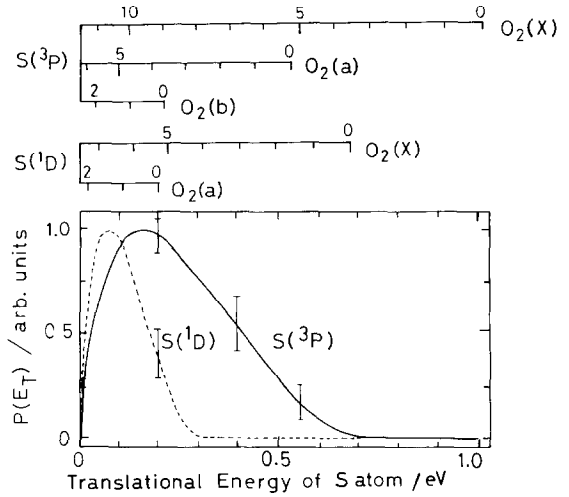

Fig. 5. Translational energy distribution of the $S(^3P)$ and $S(^1D)$ atoms obtained from fig. 3. Upper scales represent vibrational levels of the $O_2(X\,^3\Sigma^-$, $a\,^1\Delta$, and $b\,^1\Sigma_g^+)$ states, assuming molecular dissociation process, $S+O_2$. Error bars are shown by vertical lines. Below 0.1 eV, the error bars are small.

θ' in eq. (2) is 0°. The images projected on the Y axis peak at $\theta=90°$ while those projected on the X axis (or $\theta'=90°$) peak at $\theta=0°$. This is indicative of a parallel transition with respect to the velocity vector of the sulfur photofragments. The best-fit β_{obs} values are 0.42 ± 0.06 for $S(^1D)$ and 0.50 ± 0.05 for $S(^3P_2)$. The value for $S(^1D)$ is in good agreement with that obtained by the perfect focusing mass spectrometry. The anisotropy parameter for slow S atoms may be lowered by rotation of the parent molecules. If the molecule is in fact rotating, then two sorts of effects occur both of which diminish the observed β_2. First, the dissociation may not be instantaneous and has an average lifetime τ before dissociating, then, β_2 is reduced by a factor of $(1+\omega^2\tau^2)/(1+4\omega^2\tau^2)$ where ω is the angular velocity of the parent molecule. The average lifetime τ is defined by the probability $(1/\tau)\exp(-t/\tau)$ that the molecule has not dissociated in a time t [18]. Secondly, when the molecule does at last dissociate, the velocity of separation may be sufficiently low so that the molecule rotates appreciably during the dissociation. In other words, the tangential velocity of the fragments during rotation may not be negligible compared to the axial velocity of recoil, thus substantially altering their asymptotic velocity. This effect has been treated for a diatomic

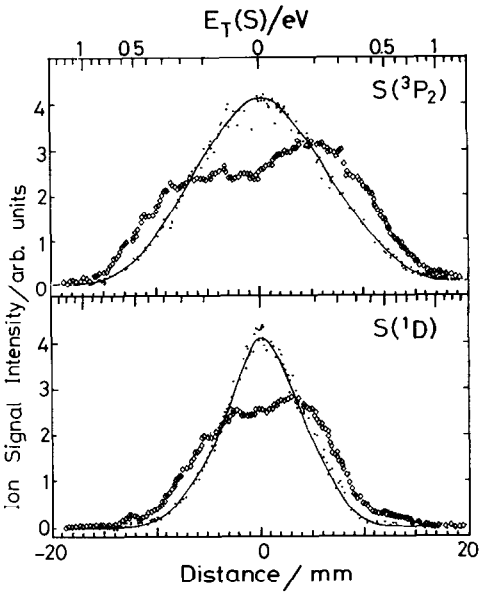

Fig. 6. Photofragment images of S(^{1}D) (bottom) and S(^{3}P) (top) following two-photon photodissociation of SO_2 at 291.49 and 308.20 nm, respectively. Dots represent the imaging intensity projected on the Y axis (perpendicular axis to the electric vector of dissociation laser light). Open squares represent the intensity projected on the X axis (parallel one). Solid lines are simulated curves assuming (a) energy distribution of the photofragment sulfur atoms of fig. 5, and (b) eq. (1) with $\beta_4=0$ and β_2 values of 0.42 for S(^{1}D) and 0.50 for S(^{3}P).

molecule that has a finite dissociation lifetime τ with the result that the anisotropy parameter β_2 becomes [19]

$$\beta_{obs}=\frac{\beta_2[P_2(\cos\alpha)+\omega^2\tau^2-3\omega\tau\sin\alpha\cos\alpha]}{1+4\omega^2\tau^2}, \quad (3)$$

$$\sin\alpha=v_t/u, \quad (4)$$

where u is the c.m. velocity and v_t the tangential velocity. The v_t vector tips the velocity vector along the dissociation axis by an angle α with respect to the molecular axis. When u is small, the angular distribution is diminished. The value of v_t is calculated to be 230 m/s for SO_2 molecules at room temperature, using $v_t=\omega r'$ where ω is the averaged angular velocity ($\omega=3.2\times10^{12}$ s^{-1}) and r', the distance of the center of mass of S from that of SO_2 ($r'=0.99$ Å) in the $\tilde{B}$ state. Table 1 shows that the average translational energy is 0.09 eV, and then, $\hat{u}$ is 740 m/s and α is 18° of S(^{1}D). Based on eq. (3) and putting the maximum value $\beta_2=2$, β_{obs} is reduced to 0.42 for $\tau=1$ ps and 1.0 for $\tau=0.1$ ps. Because of this, the observed anisotropy parameters for S(^{1}D) is taken as the lower limit.

4. Discussion

4.1. Primary processes

It has been established [20] that the threshold of the lowest channel producing S+O_2 lies at ≈210 nm. Therefore, dissociation of SO_2 in the present study does not take place with the absorption of a single 286–309 nm quantum. Indeed, it is noted that the energy of two photons corresponds to a transition to the one-photon allowed E state in SO_2 [21]. With C_{2v} symmetry approximation, a one-photon allowed state is also two-photon allowed. Thus, upon sequential absorption of two UV photons, the SO_2 molecule is endowed with sufficient energy to dissociate into a number of possible products: O_2(X, a, b)+S(^{3}P, ^{1}D) as listed in table 2. Effenhauser et al. [3] reported that excitation of SO_2 at 248 nm results in nine different primary processes that lead mostly to SO+O as well as S+O_2 fragments.

Translational energy distribution of the S atoms shown in fig. 5 suggests that the O_2 photofragments should be vibrationally excited. Because the O–O distance in SO_2 is much longer than the O–O bond lengths of O_2 (a $^1\Delta$, b $^1\Sigma_g^+$), the O_2 fragments are expected to be vibrationally excited for both the S(^{3}P) and S(^{1}D) channels based on a simple Franck–Condon model. If O_2(X) is excited up to $v=10$–11, the one-photon resonant three-photon ionization transition of O_2(B–X), (v', v'')=(0, 10), (1, 11), and (0, 11) should appear at 287.0, 292.3, and 298.4 nm, respectively. In the excitation spectrum of $m/e=32$, we observed no strong signals at these wavelengths. O_2(X, $v=10$, 11) are not formed in the S(^{3}P)+O_2(X) process. Our tentative conclusion regarding the primary process is that S atoms are accompanied by mostly O_2(a $^1\Delta_g$) and O_2(X $^3\Sigma_g^-$), and that O_2(X) is not vibrationally excited to $v=10$–11. This tentative conclusion is supported by the time-of-flight spectra of $m/e=32$ signals from two-photon

dissociation of SO_2 at 248 nm by Effenhauser et al. [3]. Their time-of-flight spectra show sharp tresholds for $S(^1D)+O_2(a\,^1\Delta)$ and $S(^3P)+O_2(a\,^1\Delta)$, which are accompanied by slow and strong time-of-flight signals.

We have tested the assertion of the photodissociation of SO photofragments as a source of the S atoms by introducing $SOCl_2$ into the chamber housing of our mass spectrometer. Since no S^+ signals were observed, SO photofragments would not be a source of the S atoms. Here, based on the thermodynamics of SO dissociation, the assertion of SO photodissociation will be discussed. According to Effenhauser et al. [3], two-photon dissociation of SO_2 at 248 and 308 nm results in mostly $SO(X\,^3\Sigma^-$ and $a\,^1\Delta)+O(^3P$ and $^1D)$. These SO photofragments may absorb additional one or two photons at 308.20 nm (4.0 eV) and 291.49 nm (4.25 eV) after two-photon dissociation of SO_2.

$$SO(X\,^3\Sigma^-)\rightarrow S(^3P)+O(^3P),\quad \Delta H=5.36\text{ eV},$$
$$\rightarrow S(^1D)+O(^3P),\quad \Delta H=8.48\text{ eV};$$
$$SO(a\,^1\Delta)\rightarrow S(^3P)+O(^3P),\quad \Delta H=4.57\text{ eV},$$
$$\rightarrow S(^1D)+O(^1D),\quad \Delta H=7.69\text{ eV}.$$

In one-photon dissociation of vibrationally excited $SO(a\,^1\Delta)$ molecules at 308.20 nm, $S(^3P)$ atoms would have very small translational energies, while fig. 5 shows that $S(^3P)$ has the maximum energy of 0.70 ± 0.05 eV, and hence $S(^3P)$ would not be formed from the one-photon dissociation of $SO(a\,^1\Delta)$. Since the laser intensity is reduced so as to obtain only a few tenths of ions per laser shot, two-photon dissociation of SO would not occur. Even if two-photon dissociation of SO(X) occurs or SO(a) produces $S(^3P)$, this atom would have a minimum translational energy of 0.88–1.14 eV. This is not the case in the present experiment.

Three-body dissociation into $S(^1D$ and $^3P)+O+O$ requires three photons at 308.2 nm as well as 291.49 nm. This three-photon process contributes to the formation of S atoms less than the two-photon process $S+O_2$ because the laser intensity in the present experiment is reduced so as to count only a few tenths of ions per laser shot. Although the formation of the O atom was reported by Effenhauser et al. [3] in the two-photon dissociation of SO_2 at 248 and 308 nm, they attributed it to the primary process SO+O. In order to obtain some information on dissociation processes, we applied the model of Baer et al. [22] to the three body dissociation. As reported by Dujardin et al. [23], there are three models, (i) the simultaneous fragmentation statistical model, (ii) the sequential fragmentation statistical model, and (iii) the classical impulsive model. In the simultaneous fragmentation statistical model (i), translational energy of the sulfur atom is given by $E_{excess}/4$, which yields 0.27 eV for $S(^3P)+2O(^3P)$ and 0.17 eV for $S(^1D)+2O(^3P)$. In the classical impulsive model (iii), E_T is given by $0.2\times E_{excess}$, which yields 0.21 eV for $S(^3P)+2O(^3P)$ and 0.13 eV for $S(^1D)+2O(^3P)$. These values are in reasonable agreement with the averaged translation energies obtained in our experiment, 0.21 eV for $S(^3P)$ and 0.09 eV for $S(^1D)$. In the sequential fragmentation statistical model (ii), the translational energy depends on the internal state of the SO photofragments. A very simple case, $SO_2\rightarrow SO(X,\ v=0,\ j=0)+O(^3P)$, $SO(X)\rightarrow S(^3P)+O(^3P)$, predicts that the $S(^3P)$ fragment has 0.65 eV as a translational energy, which is too large compared to the observed value, 0.21 eV. Other cases for model (ii) also expect a too small or a too large value as an averaged translational energy. Dujardin et al. [23] measured the translational energy of S^+ ions as a function of the incident VUV photon energy in the three-body dissociation of SO_2^+ generated from VUV irradiation of SO_2. Their results favors the simultaneous dissociation model (i) rather than the sequential dissociation model (ii), based on averaged values of the S^+ translational energy. In our SO_2 dissociation, on the basis of the average energies of the S atoms, the simultaneous dissociation model (i) could be one of possible dissociation processes. However, this process requires three photons and hence would be less probable than the two-photon dissociation processes, $SO_2\rightarrow S+O_2$.

4.2. Phototransitions of SO_2

The angular distributions of the S photofragments from SO_2 in figs. 3 and 4 are attributable mostly to a parallel optical transition. Hamada and Merer [24] carried out a rotational analysis of the vibrational bands of SO_2 between 300 and 330 nm. The bands correspond to the b_2 vibrational levels of the $\tilde{A}\,^1A_2$ electronic state. The anomalous vibrational intensity

distribution indicates that the $\tilde{A}\,^1A_2$ state undergoes strong vibronic coupling with the $\tilde{B}\,^1B_1$ electronic state. The progression forms a series of well defined features starting at 313.1 nm. These have the same strongly red degraded rotational structure, indicating a large decrease of bond angle upon electronic excitation. The geometry of the excited state is, therefore, conductive to the formation of molecular oxygen and the simultaneous breaking of the two S–O bonds. The strong continuum in the absorption spectrum below 300 nm belongs to the $\tilde{B}\,^1B_1$–$\tilde{X}\,^1A_1$ transition and the (0, 0) band is placed between 310 and 316 nm. Hiller [26] associated this band with the $(3b_1)\leftarrow(8a_1)$ transition and assigned the $(3b_1)\pi$ orbital to a S–O antibonding and an O–O bonding orbital.

In the present two-photon dissociation of SO_2 at 286–309 nm, the intermediate $\tilde{B}\,^1B_1$ state is generated after the first one-photon absorption, which has a relatively long lifetime compared to the nanosecond laser pulse. Therefore, the photodissociation dynamics are determined solely by the second transition from the intermediate $^1B_1$ state to the higher dissociative state. The vibrational band at 124 nm corresponds to the $v=4$ excitation of the bending mode of SO_2 [25]. It has been reported [6] that $S(^3P)$ and $S(^1D)$ were among the primary photofragments of SO_2 at 124 and 117 nm.

For the two-photon absorption via real intermediate state, an angular distribution of the photofragment (eq. (1)) depends not only on the symmetries of the final state but also on the lifetime of the intermediate state. That is, the angular distribution is well represented only by the second degree Legendre polynomial when the lifetime is long for the intermediate level. The contribution of the fourth degree Legendre polynomial becomes appreciable when the lifetime is short. In order to test these expectations, we have previously photodissociated CS_2 via a two-photon process at 308 nm [27]. By the first one-photon absorption, CS_2 is excited to the $^1B_2$ state with C_{2v} symmetry. Absorption of the second photon competes with the slow radiative decay of $CS_2(^1B_2)$ which has a lifetime on the order of microseconds. In this case, the experimental angular distribution is well represented by the second degree Legendre polynomial. In the present experiment, the $SO_2(^1B_1)$ intermediate state also undergoes slow radiative decay. Hence, the angular distribution is well represented by an appropriate anisotropy parameter β_2 for the second photon transition.

Table 3
Calculated anisotropy parameters for sequential two-photon dissociation of SO_2 in the transition $\tilde{X}\,^1A_1\rightarrow\tilde{B}\,^1B_1\rightarrow$ final state via the intermediate $\tilde{B}\,^1B_1$ state

Symmetry of the final state	μ [a]	χ [b] (deg)	β_2 [c]
A_1	$x\,(B_1)$	90	−1
A_2	$y\,(B_2)$	90	−1
B_1	$z\,(A_1)$	0	2

[a] Directions (symmetries) of the transition moment. The y axis lies along the 0–0 direction of SO_2.
[b] Angles between dissociation direction and transition moment. Dissociation direction is assumed to be along the C_{2v} axis (z).
[c] Anisotropy parameters of the angular distribution of the S atoms assuming symmetric dissociation of SO_2 into $S+O_2$ by second photon absorption.

Table 3 shows the calculated β_2 values based on the assumption that (a) the $\tilde{B}\,^1B_1$ state is the intermediate state for the two-photon transition, (b) the angular distribution of photoproducts reflects solely the direction of the transition moment for the second photon transition with respect to the photofragment velocity vector and (c) the photofragment sulfur atoms are separated along the C_{2v} axis of SO_2. From table 3 it is obvious that only the transition for $B_1\leftarrow B\,^1B_1$ has a positive β_2 value and is in agreement with our experimental results, that is, $\beta_2\geqslant 0.42\pm 0.06$ for $S(^1D)$, and $\beta_2\geqslant 0.50\pm 0.05$ for $S(^3P)$.

In our experiment, the two-photon excited states are in the region of 8.0–8.5 eV. Vuskovic and Trajmar [21] reported in their electron impact experiment that the angular behavior of the scattered electron of the 8.4 eV band is forward peaking and is apparently dominated by overlapping optically allowed transitions, that is, A_1, B_1, and B_2 in the C_{2v} symmetry. The B_1 assignment is in agreement with our experimental result for the two-photon excited state around 8.5 eV.

Acknowledgement

This work is partly supported by a Grant-in-Aid from the Ministry of Education, Science and Culture of Japan and the Mitsubishi Foundation. TS thanks

the JSPS Fellowship for Japanese Junior Scientists.

References

[1] M.W. Wilson, M. Rothchild, D.F. Muller and C.K. Rhodes, J. Chem. Phys. 77 (1982) 1837.
[2] T. Venkitachalam and R. Bersohn, J. Photochem. 26 (1984) 65.
[3] C.S. Effenhauser, P. Felder and J.R. Huber, Chem. Phys. 142 (1990) 311.
[4] A. Freedman, S.C. Yang and R. Bersohn, J. Chem. Phys. 70 (1979) 5313.
[5] M. Kawasaki and H. Sato, Chem. Phys. Letters 139 (1987) 585.
[6] C. Lalo and C. Vermeil, J. Photochem. 1 (1973) 321; 3 (1975) 441.
[7] M. Kawasaki, H. Sato, A. Fukuroda, T. Kikuchi, S. Kobayashi and T. Arikawa, J. Chem. Phys. 86 (1987) 4431.
[8] M. Kawasaki, H. Sato, S. Kobayashi and T. Arikawa, Chem. Phys. Letters 146 (1988) 101.
[9] M. Kawasaki, H. Sato, T. Kikuchi, S. Kobayashi and T. Arikawa, J. Chem. Phys. 87 (1987) 5739.
[10] D. Chandler and P. Houston, J. Chem. Phys. 87 (1987) 1445;
J.W. Thoman, D.W. Chandler, D.H. Parker and M.H.M. Jansen, Laser Chem. 9 (1988) 27.
[11] T. Kinugawa and T. Arikawa, J. Chem. Phys. 96 (1992) 4801; Rev. Sci. Instr. (1992), in press.
[12] G. Iwata, Progr. Theoret. Phys. 8 (1952) 183; 9 (1953) 97.
[13] T. Arikawa, Japan. J. Appl. Phys. 2 (1963) 420.
[14] W.H. Smith, J. Quant. Spectry. Radiative Transfer 9 (1969) 1191.
[15] M. Kawasaki, K. Kasatani, H. Sato, H. Shinohara and N. Nishi, Chem. Phys. 88 (1984) 135.
[16] J. Steadman and T. Baer, J. Chem. Phys. 91 (1989) 6113.
[17] R. Sander and K. Wilson, J. Chem. Phys. 63 (1975) 4242.
[18] C. Jonah, J. Chem. Phys. 55 (1971) 1915.
[19] G.E. Busch and K.R. Wilson, J. Chem. Phys. 56 (1972) 3638.
[20] H Okabe, J. Am. Chem. Soc. 93 (1971) 7095.
[21] L. Vuskovic and S. Trajmar, J. Chem. Phys. 77 (1982) 5436.
[22] T. Baer, A.E. DePrists and J.J. Hermans, J. Chem. Phys. 76 (1982) 5917.
[23] G. Dujardin, T. Govers, S. Leach and D. Winkoun, Photophysics and photochemistry above 6 eV, F. Lahmani, ed. (Elsevier, Amsterdam, 1985).
[24] Y. Hamada and A.J. Merer, Can. J. Phys. 53 (1975) 2555.
[25] I.W. Watkins, J. Mol. Spectry. 29 (1969) 402.
[26] I.H. Hiller, Mol. Phys. 22 (1971) 193.
[27] M. Kawasaki, H. Sato, T. Kikuchi, A. Fukuroda, S. Kobayashi and T. Arikawa, J. Chem. Phys. 86 (1987) 4425.
[28] J. Steadman and T. Baer, J. Chem. Phys. 89 (1988) 5507.